DOI: 10.15825/1995-1191-2025-4-183-195

IMAGE-BASED CLUSTERING ANALYSIS OF CALCIFICATION PATTERNS IN BIOPROSTHETIC HEART VALVES

E.A. Ovcharenko, K.Yu. Klyshnikov, P.S. Onishchenko, A.E. Kostyunin, A.A. Khromov, A.N. Stasev, T.N. Akentyeva, M.P. Fokeeva, O.L. Barbarash, T.V. Glushkova

Research Institute for Complex Issues of Cardiovascular Diseases, Kemerovo, Russian Federation

Objective: to identify key patterns of calcification in explanted bioprosthetic heart valves (BHVs) using cluster analysis of computed tomography-derived graphical data. **Materials and methods.** The study included 11 UniLine BHVs that were routinely explanted during reoperations for structural valve dysfunction. Computed tomography was used to obtain DICOM images of each sample, followed by generation of maximum intensity projections and segmentation of the valves into individual leaflets (n = 33). The images were pre-processed using binary thresholding to differentiate calcified regions from non-calcified biological tissue. Cluster analysis was performed using various algorithms: Gaussian mixture models, Ordering Points To Identify the Clustering Structure (OPTICS), k-means clustering, agglomerative (hierarchical) clustering, and spectral clustering. A basic quantitative method assessing the proportion of pixels corresponding to calcified areas was used for comparison. The performance of clustering algorithms was evaluated using the silhouette score. The presence of calcium deposits in the valves and the accuracy of binary thresholding were further verified histologically by alizarin red S staining of valve cryosections. **Results.** Data preprocessing based on image binarization yielded a maximum silhouette score of 0.55. Among the clustering algorithms, the highest silhouette scores were achieved with the agglomerative (0.55) and k-means (0.54) methods; however, both demonstrated substantial data imbalance, with up to 85% of samples grouped within a single cluster, limiting their practical applicability. The most balanced clustering was achieved using spectral clustering (silhouette score 0.45) and the basic quantitative approach (0.44). Both methods identified three distinct patterns of bioprosthetic valve leaflet calcification: (1) non-calcified leaflets, (2) partial calcification, and (3) total calcification. **Conclusion.** Three key calcification patterns were identified in explanted BHVs – absence of calcium, partial calcification, and total calcification. Spectral clustering and the basic quantitative method demonstrated the most balanced results, while other algorithms showed pronounced cluster imbalance. Heat map analysis revealed that in partial calcification, mineral deposition typically begins in the commissural and dome regions of the leaflets, near the free edge, and in total calcification, extends across the entire dome and leaflet base.

Keywords: bioprosthetic heart valves; prosthetic valve dysfunction; structural valve degeneration; calcification; cluster analysis.

INTRODUCTION

The introduction of bioprosthetic heart valves (BHVs) has been a major advancement in treating valvular heart disease. Owing to their physiological hemodynamic performance and the absence of a need for long-term anticoagulant therapy, BHVs are widely used in clinical practice. In 2022, 2,526 surgical and 1,633 transcatheter BHVs were implanted in the Russian Federation [1, 2]. However, their long-term durability remains a limitation due to structural valve degeneration, which ultimately leads to hydrodynamic failure. Literature reports indicate that within 10–15 years, up to half of BHVs made from xenopericardial material develop dysfunction [3]. Such cases necessitate repeat valve replacement, a procedure associated with significantly higher risks of serious complications and mortality compared with primary interventions [4–6].

In more than half of cases, calcification of the valve apparatus is the primary cause of BHV dysfunction [7]. Calcium deposition in the leaflets increases their stiffness, leading to characteristic clinical manifestations such as a high transprosthetic gradient, elevated flow velocity, and a reduced effective orifice area [8, 9].

Bioprosthetic tissue mineralization is a multifactorial process driven by the interplay of several mechanisms. These include passive calcium deposition on residual donor cells, chemically cross-linked collagen, and damaged elastic fibers, as well as active biomineralization involving apoptotic immune cells and circulating recipient factors [10]. Cyclic mechanical loading further accelerates calcification by inducing fatigue damage in collagen fibers, thereby creating sites susceptible to mineral deposition [11].

Current research actively investigates the causes and biomechanical consequences of BHV calcification to

Corresponding author: Evgeny Ovcharenko. Address: 6, Akademika Leonida Barbarasha bul'var, Kemerovo, 650002, Russian Federation.
Phone: (3842) 34-53-77. E-mail: ovchea@kemcardio.ru

develop strategies that extend their functional lifespan. One approach to elucidating calcification mechanisms involves analyzing characteristic regions and patterns of mineral deposition within valve structures. Such studies can identify areas most prone to mineralization, their relationship with mechanical stress, and potential directions for improving prosthesis design.

Existing literature presents two contrasting perspectives. Some studies demonstrate distinct and reproducible calcification patterns correlated with regions of high hemodynamic and mechanical stress [12–15] or draw analogies with native valve calcification patterns applicable to BHVs [16, 17]. Others, however, report a random distribution of mineral deposits, focusing solely on the extent and severity of calcification without defining its spatial organization [18, 19]. Both viewpoints are supported by qualitative and quantitative evidence, making it difficult to establish a unified concept of calcification distribution in BHVs.

This study aims to enhance understanding of the characteristic patterns of calcium deposit localization in explanted BHVs treated with ethylene glycol diglycidyl ether, using cluster analysis of computed tomography (CT)-derived graphical data.

MATERIALS AND METHODS

Data acquisition and preparation

The study was based on DICOM images of explanted BHVs obtained using multislice computed tomography (MSCT) on a LightSpeed™ VCT 64 scanner (General Electric, USA). All samples were mounted on a stage and scanned under the following parameters: tube voltage – 120 kV, current – 160 mA, rotation time – 0.9 s, total scan time – 6.8 s, and scan speed – 39.37 mm/rev. Image reconstruction was performed with a slice thickness of 0.625 mm using a standard reconstruction kernel.

Table 1

Clinical characteristics of patients from whom explanted bioprosthetic heart valves were obtained

Parameter	Value
Age at the time of valve replacement, median [Q1; Q2], years	57 [44.75; 65.75]
Gender:	
Male, n (%)	6 (55%)
Female, n (%)	5 (45%)
Reason for valve replacement:	
Structural valve degeneration, n (%)	6 (55%)
Prosthetic endocarditis, n (%)	5 (45%)
Coexisting diseases:	
Hypertensive disease, n (%)	3 (27%)
Dyslipidemia, n (%)	2 (18%)
Diabetes mellitus, n (%)	1 (9%)
Chronic kidney disease, n (%)	7 (64%)
Prosthesis functioning period, median [Q1; Q2], years	2.75 [0.79; 5.90]

A total of 11 Uniline xenopericardial atrioventricular BHVs were analyzed. These prostheses had been routinely explanted and replaced at the Research Institute for Complex Issues of Cardiovascular Diseases in Kemerovo, Russia between 2015 and 2024. A brief clinical description of the patients is provided in Table 1.

The DICOM images obtained were processed as maximum intensity projections (MIP) in a top-view orientation. Each prosthesis image was then manually segmented into three leaflets and aligned into a unified position to achieve an overlay of all leaflets from the 11 samples (Fig. 1).

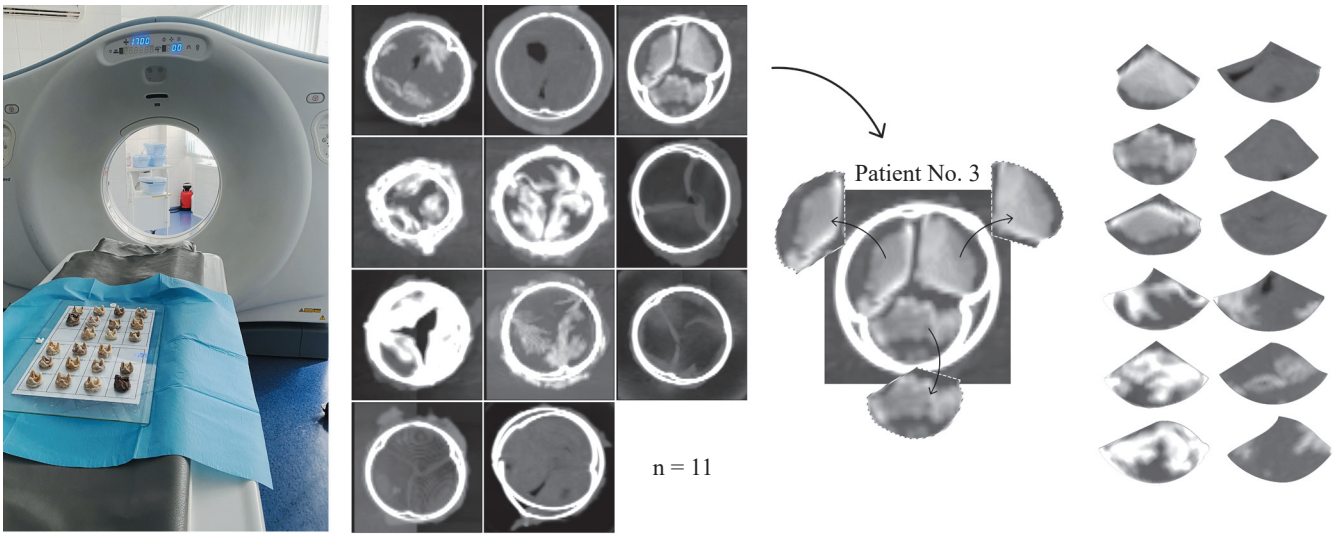

Fig. 1. Workflow for obtaining input data for the segmentation algorithm. An enlarged sequence is presented, from CT scanning of the explanted bioprosthetic heart valves to obtaining images of individual valves used for clustering

The resulting dataset – comprising 33 individual leaflets represented as separate images – was subjected to cluster analysis using various data preprocessing strategies and clustering algorithms.

Data preprocessing strategies

Three preprocessing strategies were applied:

1) **Raw data:** Processing of raw DICOM images without any modifications.
2) **Image binarization to identify calcified regions** (calcified tissue only). A binary thresholding method was applied, where pixels with an intensity range of 193–255 were assigned a value of 255, and all others were set to 0. This approach enabled clear identification of calcified regions, which is clinically relevant for assessing valve degeneration.
3) **Combined representation** (calcified and non-calcified tissue): In this approach, pixels were differentiated in a more detailed way. Pixels with intensities from 193 to 255 were set to 255 (indicating calcification), while those from 1 to 192 were set to 124 (representing non-calcified biomaterial). This strategy allowed for simultaneous highlighting of calcified and soft tissue areas, which facilitated a more detailed analysis of the images obtained.

Clustering algorithms

Basic method. This approach served as a reference (comparison) method. Clustering was performed artificially based on calcium levels. All images were binarized using a threshold of 193/255, after which the number of white pixels – corresponding to areas of valve mineralization – was calculated. The median and quartile values of this parameter were then determined. Based on these statistics, three clusters were defined: low calcification (images with calcium content below the median); medium (images within the third quartile [50–74% of the sample]; high calcification (images within the fourth quartile [75–100% of the sample]).

The following clustering algorithms were applied in the study:

1) **Gaussian Mixture Models (GMM).** This probabilistic model was selected for its ability to represent data as a combination of probability distributions, allowing estimation of intra-cluster variance. GMM is well suited for heterogeneous image datasets, particularly when clusters overlap or have uneven density [20].
2) **Ordering Points to Identify the Clustering Structure (OPTICS).** OPTICS was used to detect clusters of arbitrary shape under conditions of variable data density. Its robustness makes it effective for analyzing fragmented or irregular structures, such as those found in medical images affected by artifacts or low signal-to-noise ratios [21].
3) **k-Means Method.** The k-means algorithm was chosen for its computational efficiency and scalability, which are advantageous in large-scale image segmentation. Although it assumes spherical cluster geometry, its simplicity and established performance in image analysis justify its inclusion in the study [20].
4) **Agglomerative Clustering.** This hierarchical approach was employed to uncover nested structure within the data, enabling a detailed examination of images with multi-scale structural patterns [22].
5) **Spectral Clustering.** This algorithm was applied to identify complex, non-spherical data structures. Its effectiveness in separating non-linearly separable clusters has been confirmed in a number of studies [22].

Indicators analyzed

The study evaluated several quantitative and qualitative indicators to evaluate the performance of the clustering algorithms.

1) **Silhouette score:** This metric, ranging from –1 to +1, was used to assess cluster compactness and separability. Values close to +1 indicate well-defined, cohesive clusters with minimal overlap, while negative values suggest incorrect or ambiguous data partitioning [23].
2) **Clustered image grouping with label display.** Images assigned to each cluster were organized in matrix form with corresponding textual labels. This visualization enabled qualitative assessment of cluster semantic consistency, detection of anomalies, and analysis of object distribution within groups.
3) **Principal component analysis (PCA) visualization.** PCA was employed for linear dimensionality reduction, allowing the data to be represented in a two-dimensional (2D) space. This facilitated assessment of data dispersion and cluster separability.
4) **t-distributed stochastic neighbor embedding (t-SNE) visualization.** Nonlinear dimensionality reduction using t-SNE [24] was applied to visualize clusters with complex, non-linear structures while preserving local relationships between points. The results were compared with PCA visualizations to assess the stability of the identified clustering patterns.
5) **Maximum intensity projections (MIP).** To evaluate the spatial distribution of calcifications, all image slices (frames) were combined into a single 2D projection by selecting the maximum pixel intensity values along the Z-axis.
6) **Heat map of relative cumulative calcium distribution.** Using normalized pixel intensities (range [0–1]), aggregated maps of calcification density were generated for both the overall dataset and individual clusters. This visualization highlighted probabilistic differences in the density and spatial organization of calcifications between groups.

The technical implementation of preliminary data processing, clustering analysis, and data visualization

was carried out in the Python 3.11 programming environment using the OpenCV, NumPy, Pandas, and Scikit-learn libraries. The complete program code is available at: https://github.com/Eugene-Ovcharenko/BHV_leaflet_images_clustering.git.

Visualization of calcium using histological methods

The study results were validated through histological analysis. After MSCT scanning, the valve leaflets were carefully separated from the BHV frame to prepare histological sections. Fragments of the biomaterial were fixed in Neg-50 rapid tissue freezing medium (6502, Thermo Fisher Scientific, USA), and serial cryosections were obtained using an HM525 microtome-cryostat (Thermo Fisher Scientific, USA). The resulting sections, 5 μm thick, were placed on microscope slides.

Calcium deposits were visualized by staining the sections with Alizarin Red S (ab142980, Abcam) according to the manufacturer's instructions. The stained sections were examined under a Meiji Techno MT5300L automated laboratory biological microscope, and subsequent image processing was performed using QuPath 0.4.1 software.

RESULTS

In total, this study produced 325 clustering variants of MSCT data, combining different image preprocessing strategies, clustering algorithms, variable cluster numbers (ranging from 2 to 5), and algorithm-specific hyperparameters. Given the exploratory nature of the analysis, the results were evaluated sequentially according to: data preprocessing strategies, clustering algorithms, and the most effective combinations of both.

Data preprocessing strategies

All preprocessing approaches had a marked impact on the analyzed imaging data (Fig. 2a). Image binarization on calcium intensity threshold, visualized using principal component analysis (Fig. 2b), revealed some distinguishable regions that could be further separated into distinct groups. However, most data points overlapped due to the predominance of empty (non-calcified) areas after binarization.

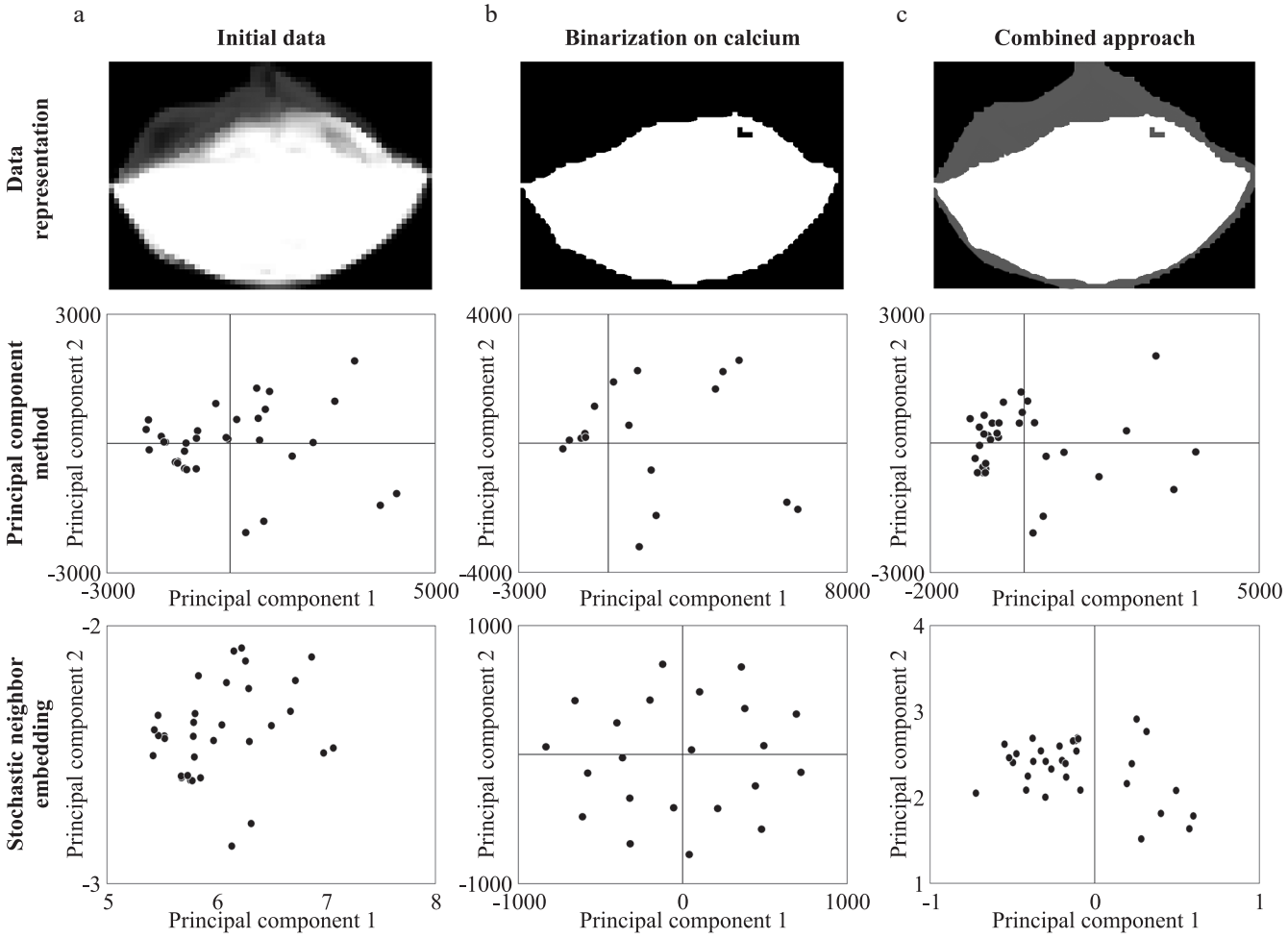

Fig. 2. Visualization of different data preprocessing strategies. Shown are examples of maximum intensity projection (MIP), principal component analysis (PCA) visualization, and t-distributed stochastic neighbor embedding (t-SNE) visualization applied to images of bioprosthetic valve leaflets

The combined option, consisting of a combination of binarized data on calcium threshold and biomaterial threshold, also provided clearer separation and superior visualization when analyzed using t-SNE (Fig. 2c).

Importantly, histological examination of the BHV leaflets confirmed the accuracy of the image binarization results: the locations of macrocalcifications observed in histological sections corresponded closely with the mineralization patterns identified from the processed MSCT images (Fig. 3).

Quantitative analysis of the clustering results across the three preprocessing strategies revealed that only one approach – image binarization based on the calcium threshold – produced satisfactory silhouette scores (Table 2). This method achieved a score of 0.55, which is considered high within the possible range of –1 to +1.

Clustering algorithms

Analysis of the results revealed a marked variation in clustering quality depending on the algorithm used (Table 3). The OPTICS algorithm proved ineffective in this context, showing an extremely low silhouette score close to zero. Other algorithms performed better, achieving silhouette scores in the range of 0.54–0.55 in the best cases. However, in most instances, the resulting clusters were highly unbalanced. Specifically, algorithms with higher silhouette scores consistently produced one dominant cluster (Class I) and two much smaller clusters (Classes II and III), comprising only 3–18% of the dataset. This pronounced imbalance indicates that the observed groupings likely do not reflect distinct patterns of calcification.

Among all the results presented, two configurations stood out: No. 0346 (Basic) and No. 0159 (Spectral) (Table 3). Both demonstrated moderate silhouette scores of 0.44 and 0.45, respectively, with a relatively balanced class distribution. In these cases, the primary class comprised 52% and 64% of the images, respectively, while Classes II and III included 15–24% of the dataset. Overall, these results indicated the presence of distinct

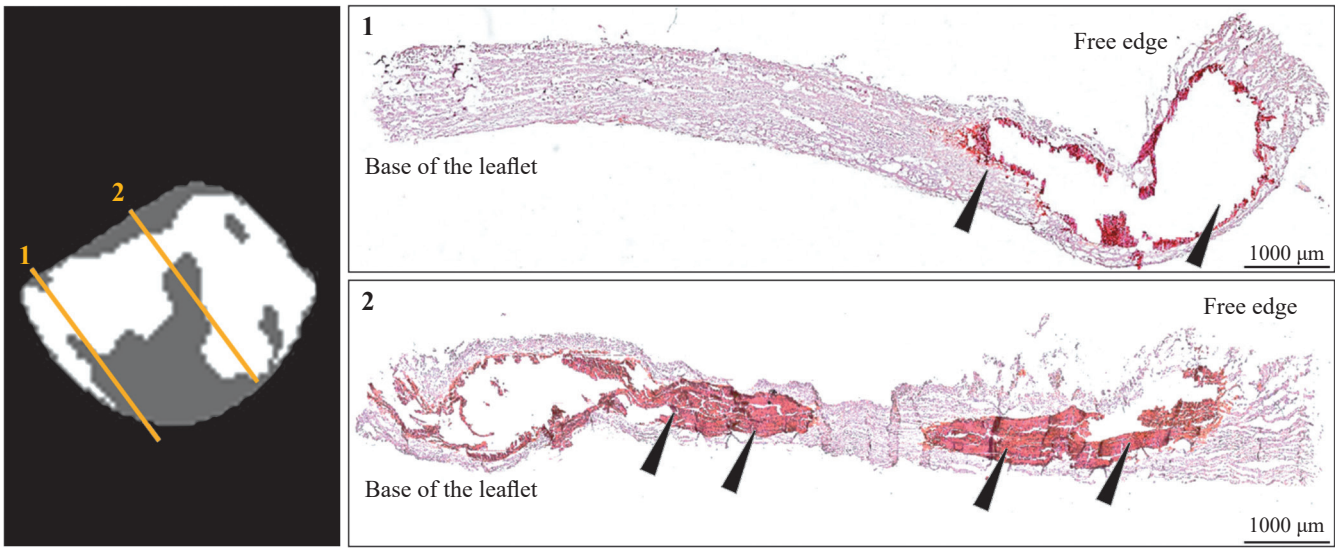

Fig. 3. Comparison between the binarized image of the valve and the corresponding histological section stained with alizarin red S. Arrows indicate areas of calcium deposition

Table 2

Quantitative characteristics of clustering algorithms, grouped by data preprocessing strategy

No.	Strategy	Number of clusters	Silhouette score	Cluster I size, %	Cluster II size, %	Cluster III size, %
0043	Initial data	3	0.37	91	6	3
0042	Initial data	3	0.33	12	82	6
0041	Initial data	3	0.30	58	30	6
0159	Binarization	3	0.55	9	85	6
0346	Binarization	3	0.55	9	85	6
0166	Binarization	4	0.54	85	6	6
0274	Combined	3	0.08	21	58	21
0273	Combined	3	0.07	21	33	45
0271	Combined	3	0.07	21	24	55

Note: For clarity, the table includes only the three preliminary data preprocessing strategies that achieved the best silhouette scores. All other configurations demonstrated significantly lower performance.

calcification classes. The clustering outcomes of these two algorithms (No. 0346 and No. 0159) are illustrated in Fig. 4, showing the division of the dataset into separate classes corresponding to specific calcification patterns. Qualitative analysis revealed that both methods identified three main heterogeneous groups: absence of calcium, partial calcification, and total calcification. It is worth noting that the spectral method misclassified five images exhibiting partial calcification into Cluster I (absence of calcium), which slightly distorted the result.

The next phase of the study involved merging the individual images associated with each cluster to form representative calcification patterns. These patterns were grouped into three categories: no calcification, partial calcification, and total calcification of the valve (Fig. 5).

The next stage of the study involved combining individual images from each cluster into distinct calcification patterns: absence of calcium, partial calcification, and total calcification (Fig. 5). Heat maps generated using two clustering algorithms (basic and spectral) illustrated the probability distribution of mineralization within the leaflet apparatus of the BHVs. Overall, the patterns obtained by both methods were largely consistent; however, the spectral method more distinctly identified certain leaflets with low levels of calcification within cluster I, resulting in qualitative differences between the heat maps. Notably, in cluster II (partial calcification), calcium deposits were predominantly located in the commissural zone and along the valve dome near the free edge, whereas in cluster III (total calcification), they were concentrated in the central portion of the leaflet dome. The PCA diagram (Fig. 6) helps explain this phenomenon: the spectral algorithm tended to assign cluster I (no calcification) to images situated very close to those in cluster II. Thus, the heat map analysis revealed differences between clusters not only in the extent of calcification but also in its spatial distribution.

DISCUSSION

Calcification of BHVs is a multifactorial process driven by a complex interplay of material changes [10]. Research groups have extensively investigated both native heart valves [25] and their bioprosthetic counterparts [12–14] in an effort to identify clinical and metabolic predictors of this condition [26, 27]. An important method for determining the causes and characteristics of bioprosthetic calcification is the analysis of mineral deposit distribution within the valve apparatus.

According to literature reports, investigators have reached two contrasting conclusions when interpreting existing data: some describe a distinct pattern in the localization of calcium deposits, whereas others emphasize their random distribution [12–15, 28, 29]. On one hand, studies correlating calcium accumulation with regions of high mechanical or shear stress have demonstrated well-defined localization patterns [12–15]. The areas of greatest mechanical loading, primarily the valve dome and commissural zones, are therefore regarded as predisposed to mineralization. On the other hand, several authors attribute bioprosthetic calcification to the infiltration of blood-derived molecular components and subsequent immune responses to xenogeneic tissue [28, 29]. Within this framework, the entire volume of the biomaterial becomes a potential target for calcification, and it is not possible to identify a single characteristic pattern [18, 19].

Table 3

Quantitative characteristics of clustering algorithms

No.	Clustering algorithm	Number of clusters	Silhouette score	Cluster I size, %	Cluster II size, %	Cluster III size, %
0346	**Basic**	**3**	**0.44**	**52**	**24**	**24**
0138	Gaussian mixture	3	0.50	76	18	6
0136	Gaussian mixture	3	0.50	79	15	6
0137	Gaussian mixture	3	0.50	79	15	6
0113	OPTICS	3	0.04	24	18	58
0114	OPTICS	2	–0.01	24	76	–
0343	OPTICS	3	–0.08	12	18	70
0120	k-means	3	0.54	82	6	12
0121	k-means	3	0.54	82	6	12
0122	k-means	3	0.54	82	6	12
0198	Agglomerative	3	0.55	85	9	6
0199	Agglomerative	3	0.55	85	9	6
0201	Agglomerative	3	0.53	91	3	6
0159	**Spectral**	**3**	**0.45**	**64**	**15**	**21**
0162	Spectral	3	0.28	27	55	18
0163	Spectral	3	0.28	27	55	18

Note: For clarity, the table includes only the three clustering algorithms that achieved the best silhouette scores. All other algorithms demonstrated significantly lower performance. Minor classes (small cluster sizes) are highlighted in gray.

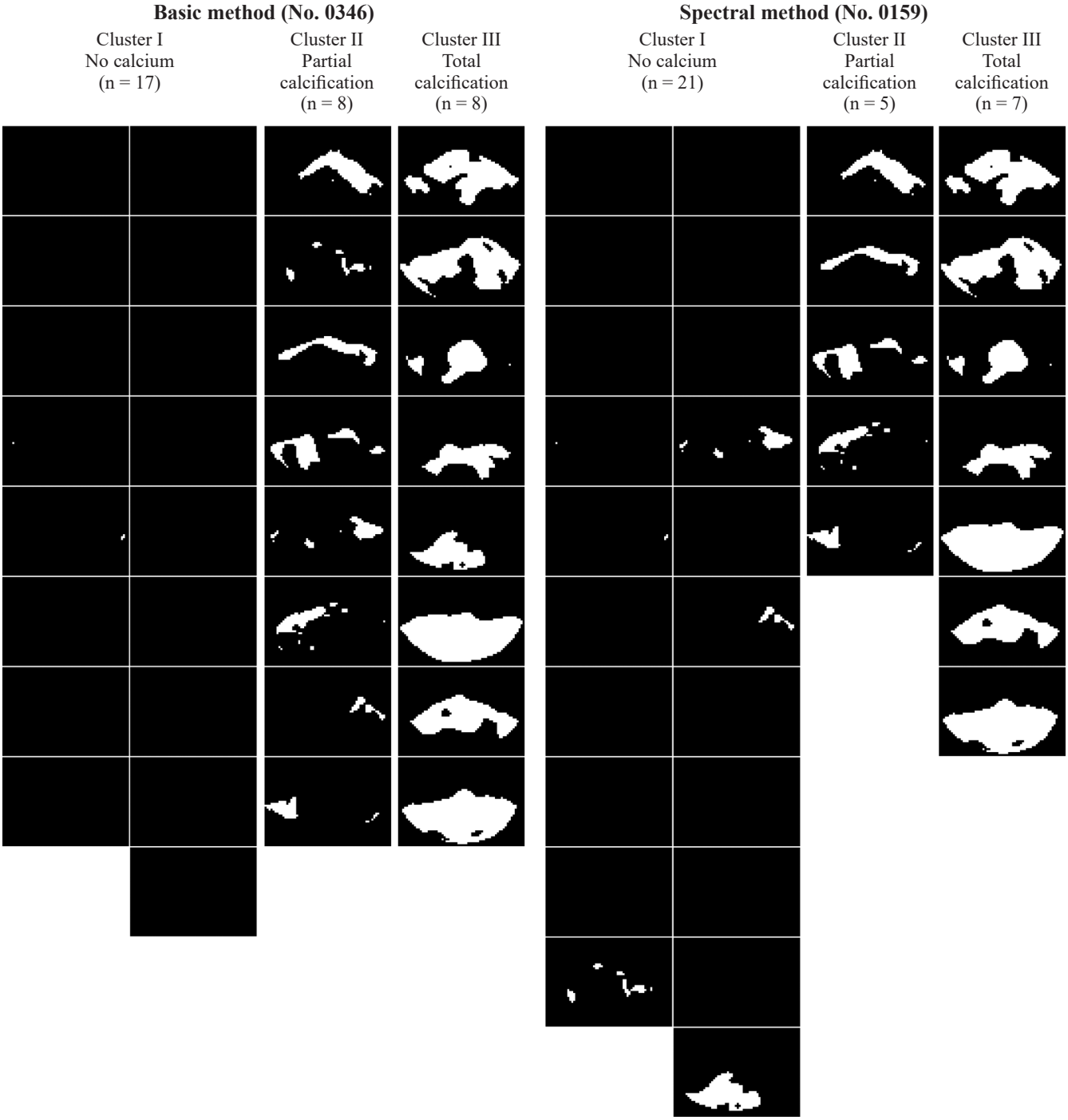

Fig. 4. Visualization of the distribution of valve images after threshold-based calcium detection. The figure illustrates the results obtained using the two most effective clustering algorithms – basic and spectral clustering. Three distinct classes are identified: absence of calcium, partial calcification, and total calcification

Our previous pilot study [30], together with the present investigation, largely supports the former hypothesis – that regions of mineralization tend to colocalize with areas of increased mechanical stress on the valve leaflets. However, the current results provide a more detailed characterization of the extent and spatial distribution of calcium deposits across different degrees of mineralization – we were able to identify the leaflet regions most frequently affected in cases of partial and total calcification.

For cluster II (partial calcification), the predominant areas of mineralization were located in the commissural region and along the valve dome near the free edge, whereas for cluster III (total calcification), calcification was concentrated in the central portion of the dome (Fig. 5). This suggests that the calcification process develops progressively – from initial involvement of the commissures and the line of coaptation to subsequent extension into the dome region.

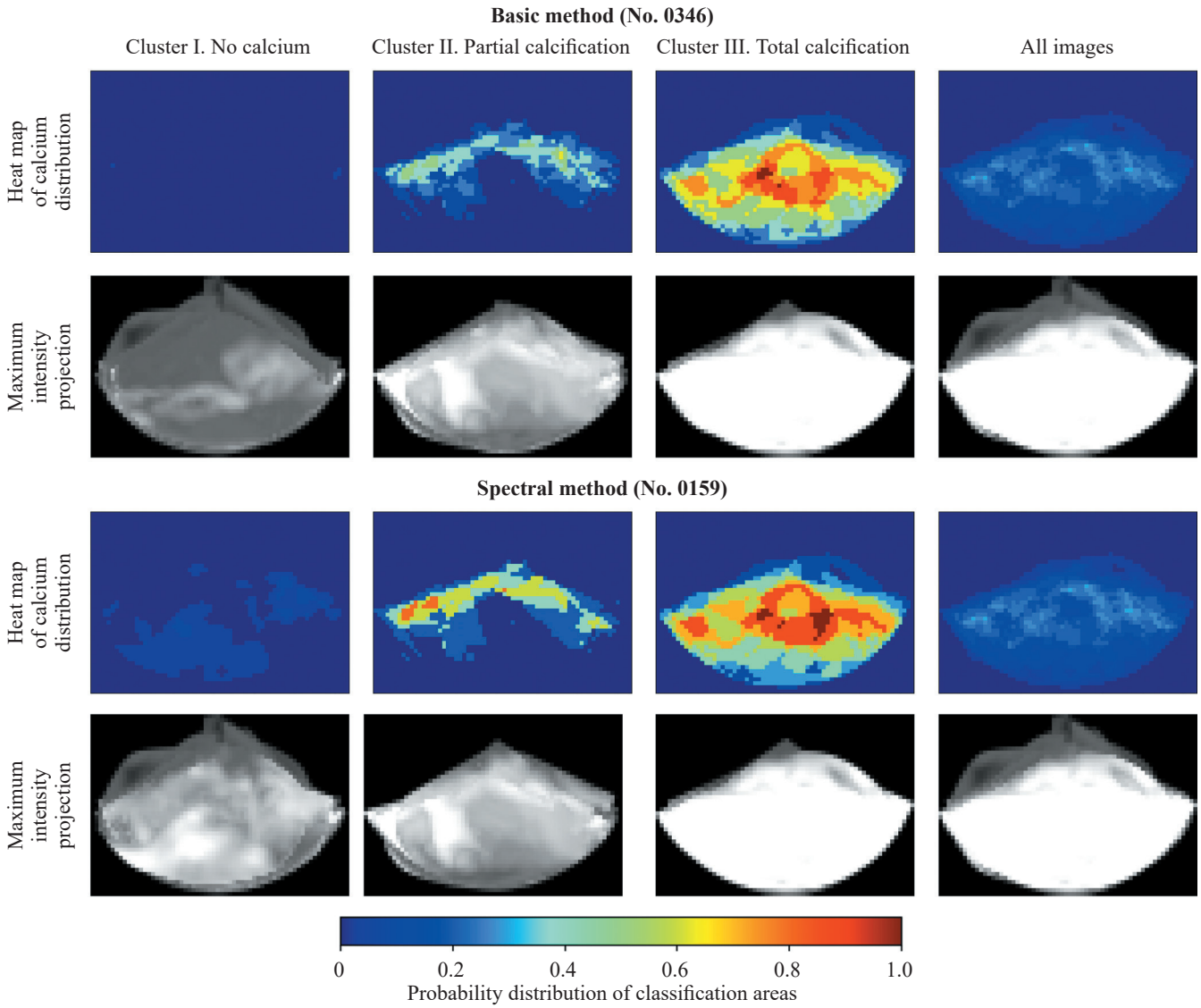

Fig. 5. Final image of calcification clusters obtained using the two most effective approaches – the basic method and the spectral clustering algorithm. The data are presented as a heat map of the relative cumulative distribution of calcium and as an overlay of all the original MSCT images

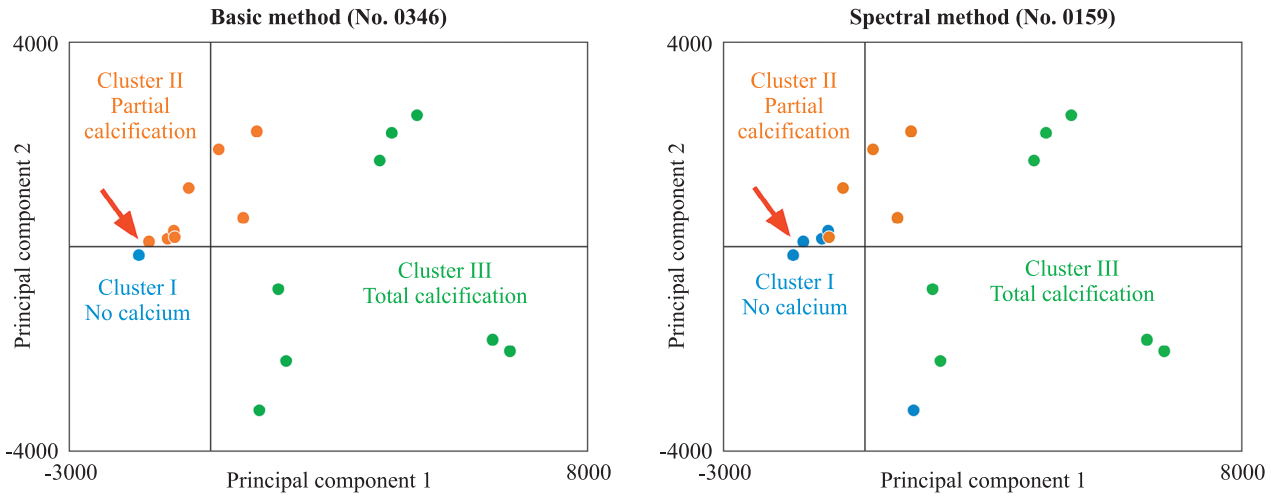

Fig. 6. Principal component analysis (PCA) diagram characterizing the identified clusters of calcification images. Results for both of the most effective algorithms are presented. The arrows indicate key differences between the two algorithms – in clusters I and II. Note: Because of point overlap, cluster I appears as a single point, as all empty images after binarization have the same coordinates within the principal component space

However, the present results do not allow this hypothesis to be confirmed, as further investigation is required.

It is noteworthy that a similar pattern of calcification was observed for both foreign (literature data) and domestic (this study) bioprostheses, despite differences in biomaterial preservation techniques. In a study by Tsolaki et al. (2023) involving Perimount Magna Ease bioprosthetic valves (n = 14) stabilized with glutaraldehyde, the valve dome was identified as the region most susceptible to calcification [12]. In the current study, domestically produced prostheses preserved with ethylene glycol diglycidyl ether exhibited comparable localization of mineralization, primarily within the dome region. This concordance likely reflects the dominant role of mechanical stress as a key factor promoting or accelerating calcification, given that the greatest stress occurs within the dome of the valve leaflet [12].

Finally, it is worth briefly highlighting the applied aspect of this study. From a practical standpoint, the identified calcification patterns make it possible to determine the most vulnerable regions of bioprosthetic valves and to outline potential directions for their structural optimization. For example, the predominant localization of calcium deposits in specific areas of the valve leaflets can be considered in the design of new biomaterials or in modifying valve geometry to reduce mechanical stress, one of the key factors contributing to prosthesis dysfunction [10–15].

From a methodological perspective, analyzing the technical component of the work revealed that data preprocessing techniques significantly influenced the quality of clustering. The most effective approach was image binarization based on a calcium intensity threshold, which yielded the highest silhouette score (0.55), reflecting clear structural differentiation among samples. In contrast, a combined preprocessing strategy – smoothing the brightness range while retaining original, non-binarized images – proved less effective. Thus, binary segmentation of pixels into calcified and non-calcified regions enhances both the accuracy of clustering and the identification of structural patterns associated with pathological changes. This result is quite expected, given that MSCT imaging of bioprostheses is primarily intended to visualize calcium deposits, which therefore serve as the principal criterion for cluster formation: the more pronounced the calcified regions, the easier it is to cluster images.

A comparison of the clustering algorithms demonstrated that the most balanced results were obtained using the spectral algorithm and the basic method. Both approaches provided satisfactory grouping of bioprosthetic valve images into three distinct classes: without calcification, with partial calcification, and with total calcification. In contrast, the Gaussian mixture model, k-means, and agglomerative clustering achieved relatively high silhouette scores but exhibited significant class imbalance, with uneven sample distribution across clusters, thereby complicating the interpretation of results.

CONCLUSION

The optimal method for preprocessing MSCT images of BHVs explanted due to dysfunction was image binarization on the threshold of calcium X-ray density, as determined by clustering quality assessment. Among the tested clustering algorithms, the spectral clustering proved to be the most effective, allowing balanced clusters to be identified based on calcium distribution.

Analysis of the calcification characteristics in BHVs explanted due to dysfunction revealed three key calcification patterns, clearly differentiated by the ratio of mineralized to intact biomaterial: non-calcified leaflets, partial calcification, and total calcification. These characteristic patterns correspond to the extent of structural alteration and are presumably localized in regions exposed to the greatest mechanical stress. Heat maps illustrating the probability of calcium localization showed that, in partial calcification, mineralization predominantly affects the commissural areas and the valve dome near the free edge, whereas in total calcification, calcium deposition extends across the entire dome region.

The authors declare no conflict of interest.

REFERENCES

1. *Bokeriya LA, Milievskaya EB, Pryanishnikov VV, Yurlov IA.* Serdechno-sosudistaya khirurgiya – 2022. Bolezni i vrozhdennye anomalii sistemy krovoobrashcheniya. M.: NMITs SSKh im. A.N. Bakuleva, 2023; 344. (In Russ.).
2. *Alekyan BG, Grigor'yan AM, Staferov AV, Karapetyan NG.* Rentgenendovaskulyarnaya diagnostika i lechenie zabolevaniy serdtsa i sosudov v Rossiyskoy Federatsii – 2021 god. *Endovaskulyarnaya khirurgiya.* 2022; 9: 1–254. (In Russ.). doi: 10.24183/2409-4080-2022-9S.
3. *Wang M, Furnary AP, Li H-F, Grunkemeier GL.* Bioprosthetic Aortic Valve Durability: A Meta-Regression of Published Studies. *Ann Thorac Surg*. 2017 Sep; 104 (3): 1080–1087. doi: 10.1016/j.athoracsur.2017.02.011.
4. *Kaneko T, Vassileva CM, Englum B, Kim S, Yammine M, Brennan M et al.* Contemporary outcomes of repeat aortic valve replacement: A benchmark for transcatheter valve-in-valve procedures. *Ann Thorac Surg.* 2015 Oct; 100 (4): 1298–1304. doi: 10.1016/j.athoracsur.2015.04.062.
5. *Klyshnikov KU, Ovcharenko EA, Stasev AN, Scheglova NA, Odarenko YuN, Khalivopulo IK et al. In vitro* study of a biological prosthetic valve for seamless fixation. *Russian Journal of Transplantology and Artificial Organs*. 2017; 19 (4): 61–69. (In Russ, English abstract). doi: 10.15825/1995-1191-2017-4-61-69.
6. *Balsam LB, Grossi EA, Greenhouse DG, Ursomanno P, Deanda A, Ribakove GH et al.* Reoperative valve surgery in the elderly: Predictors of risk and long-term survival. *Ann Thorac Surg*. 2010 Oct; 90 (4): 1195–1200. doi: 10.1016/j.athoracsur.2010.04.057.

7. *Marro M, Kossar AP, Xue Y, Frasca A, Levy RJ, Ferrari G.* Noncalcific Mechanisms of Bioprosthetic Structural Valve Degeneration. *J Am Heart Assoc*. 2021 Feb 2; 10 (3): e018921. doi: 10.1161/JAHA.120.018921.
8. *Capodanno D, Petronio AS, Prendergast B, Eltchaninoff H, Vahanian A, Modine T et al.* Standardized definitions of structural deterioration and valve failure in assessing long-term durability of transcatheter and surgical aortic bioprosthetic valves: a consensus statement from the European Association of Percutaneous Cardiovascular Interventions (EAPCI) endorsed by the European Society of Cardiology (ESC) and the European Association for Cardio-Thoracic Surgery (EACTS). *Eur Heart J*. 2017 Dec 1; 38 (45): 3382–3390. doi: 10.1093/eurheartj/ehx303.
9. *Dvir D, Bourguignon T, Otto CM, Hahn RT, Rosenhek R, Webb JG et al.* Standardized Definition of Structural Valve Degeneration for Surgical and Transcatheter Bioprosthetic Aortic Valves. *Circulation*. 2018 Jan 23; 137 (4): 388–399. doi: 10.1161/CIRCULATIONAHA.117.030729.
10. *Kostyunin AE, Yuzhalin AE, Rezvova MA, Ovcharenko EA, Glushkova TV, Kutikhin AG.* Degeneration of Bioprosthetic Heart Valves: Update 2020. *J Am Heart Assoc*. 2020 Oct 20; 9 (19): e018506. doi: 10.1161/JAHA.120.018506.
11. *Whelan A, Williams E, Fitzpatrick E, Murphy BP, Gunning PS, O'Reilly D, Lally C.* Collagen fibre-mediated mechanical damage increases calcification of bovine pericardium for use in bioprosthetic heart valves. *Acta Biomater*. 2021 Jul 1; 128: 384–392. doi: 10.1016/j.actbio.2021.04.046.
12. *Tsolaki E, Corso P, Zboray R, Avaro J, Appel C, Liebi M et al.* Multiscale multimodal characterization and simulation of structural alterations in failed bioprosthetic heart valves. *Acta Biomater*. 2023 Oct 1; 169: 138–154. doi: 10.1016/j.actbio.2023.07.044.
13. *Kim H, Lu J, Sacks MS, Chandran KB.* Dynamic Simulation of Bioprosthetic Heart Valves Using a Stress Resultant Shell Model. *Ann Biomed Eng*. 2008 Feb; 36 (2): 262–275. doi: 10.1007/s10439-007-9409-4.
14. *Halevi R, Hamdan A, Marom G, Mega M, Raanani E, Haj-Ali R.* Progressive aortic valve calcification: Three-dimensional visualization and biomechanical analysis. *J Biomech*. 2015 Feb 5; 48 (3): 489–497. doi: 10.1016/j.jbiomech.2014.12.004.
15. *Thubrikar MJ, Deck JD, Aouad J, Nolan SP.* Role of mechanical stress in calcification of aortic bioprosthetic valves. *J Thorac Cardiovasc Surg*. 1983 Jul; 86 (1): 115–125. doi: 10.1016/S0022-5223(19)39217-7.
16. *Morany A, Lavon K, Halevi R, Haj-Ali N, Bluestein D, Raanani E et al.* Fragmentation of Different Calcification Growth Patterns in Bicuspid Valves During Balloon Valvuloplasty Procedure. *Ann Biomed Eng*. 2023 May; 51 (5): 1014–1027. doi: 10.1007/s10439-022-03115-8.
17. *Luraghi G, Matas JFR, Beretta M, Chiozzi N, Iannetti L, Migliavacca F.* The impact of calcification patterns in transcatheter aortic valve performance: a fluid-structure interaction analysis. *Comput Methods Biomech Biomed Engin*. 2021 Mar; 24 (4): 375–383. doi: 10.1080/10255842.2020.1817409.
18. *Pestiaux C, Pyka G, Quirynen L, De Azevedo D, Vanoverschelde J-L, Lengelé B et al.* 3D histopathology of stenotic aortic valve cusps using *ex vivo* microfocus computed tomography. *Front Cardiovasc Med*. 2023 Apr 25; 10: 1129990. doi: 10.3389/fcvm.2023.1129990.
19. *Cartlidge TRG, Doris MK, Sellers SL, Pawade TA, White AC, Pessotto R et al.* Detection and Prediction of Bioprosthetic Aortic Valve Degeneration. *J Am Coll Cardiol*. 2019 Mar 19; 73 (10): 1107–1119. doi: 10.1016/j.jacc.2018.12.056.
20. *Bishop C.* Pattern Recognition and Machine Learning. *Journal of Electronic Imaging*. 2006 Jan; 16 (4): 140–155. doi: 10.1117/1.2819119.
21. *Ankerst M, Breunig MM, Kriegel H-P, Sander J.* OPTICS: ordering points to identify the clustering structure. *ACM SIGMOD Rec*. 1999 Jun; 28 (2): 49–60. doi: 10.1145/304181.304187.
22. *Murtagh F, Contreras P.* Algorithms for hierarchical clustering: an overview. *WIREs Data Min Knowl Discov*. 2012 Dec 7; 2 (1): 86–97. doi: 10.1002/widm.53.
23. *Rousseeuw PJ.* Silhouettes: A graphical aid to the interpretation and validation of cluster analysis. *J Comput Appl Math*. 1987 Nov; 20: 53–65. doi: 10.1016/0377-0427(87)90125-7.
24. *Van der Maaten L, Hinton G.* Visualizing High-Dimensional Data Using t-SNE. *J Mach Learn Res*. 2008; 9 (86): 2579–2605.
25. *Leong SW, Soor GS, Butany J, Henry J, Thangaroopan M, Leask RL.* Morphological findings in 192 surgically excised native mitral valves. *Can J Cardiol*. 2006 Oct; 22 (12):1055–1061.doi:10.1016/S0828-282X(06)70321-X.
26. *Rutkovskaya NV, Kagan ES, Kondyukova NV, Kuzmina OK, Barbarash LS.* Prediction of Risk of Calcification of Heart Valve Bioprostheses on the Basis of Comprehensive Assessment of Recipients Clinical Factors and Their Compliance With Therapy. *Kardiologiia*. 2018; 58 (10): 27–33. (In Russ, English abstract). doi: 10.18087/cardio.2018.10.10182.
27. *Mahjoub H, Mathieu P, Larose E, Dahou A, Sénéchal M, Dumesnil J-G et al.* Determinants of aortic bioprosthetic valve calcification assessed by multidetector CT. *Heart*. 2015 Mar; 101 (6): 472–477. doi: 10.1136/heartjnl-2014-306445.
28. *Frasca A, Xue Y, Kossar AP, Keeney S, Rock C, Zakharchenko A et al.* Glycation and Serum Albumin Infiltration Contribute to the Structural Degeneration of Bioprosthetic Heart Valves. *JACC Basic to Transl Sci*. 2020 Aug 5; 5 (8): 755–766. doi: 10.1016/j.jacbts.2020.06.008.
29. *Sakaue T, Koyama T, Nakamura Y, Okamoto K, Kawashima T, Umeno T et al.* Bioprosthetic Valve Deterioration. *JACC Basic to Transl Sci*. 2023 May 10; 8 (7): 862–880. doi: 10.1016/j.jacbts.2023.01.003.
30. *Ovcharenko EA, Klyshnikov KU, Glushkova TV, Batranin AV, Rezvova MA, Kudryavtseva YA, Barbarash LS.* Evaluation of a failed heart valve bioprosthesis using microcomputed tomography. *Sovremennye tehnologii v medicine*. 2017; 9 (3): 15–22. (In Russ.). https://doi.org/10.17691/stm2017.9.3.02.

The article was submitted to the journal on 18.06.2025